

# Micro-area X-ray diffraction measurement by SmartLab $\mu$ HR diffractometer system with ultra-high brilliance microfocus X-ray optics and two-dimensional detector HyPix-3000

Yuji Shiramata\*

## 1. Introduction

X-ray diffraction is an analytical method for the characterization of the crystalline structure of a material, where the X-ray intensity ( $I$ ) variation is recorded as a function of diffraction angle ( $2\theta$ ). The diffraction region where  $2\theta \leq 10^\circ$  is called the Small Angle X-ray Scattering (SAXS) area, and the area where  $2\theta \geq 5^\circ$  is called the Wide Angle X-ray Scattering (WAXS) or the Wide Angle X-ray Diffraction (WAXD) area. Since the X-ray diffraction method enables evaluation of various physical properties, it is widely applicable to qualitative analysis (crystal phase identification), quantitative analysis, crystal structure analysis, orientation analysis, particle size analysis and so on.

In general, with the powder X-ray diffraction method, measurement is performed by irradiating X-rays onto a large area of the sample surface, approx.  $10\text{mm} \times 2\text{--}3\text{mm}$ . On the other hand, in order to perform an analysis of a tiny sample, or to analyze something like a micro area of a rock specimen, it is necessary to narrow the X-ray irradiation field to approx.  $0.01\text{mm}\text{--}1\text{mm}$ . In the past, because these measurements used the slit collimation method to form a narrow beam by inserting a slit into the incident optical system, X-ray intensity was low and therefore measurements took a long time. However, with the latest X-ray diffractometers, which take advantage of the remarkable progress in technology for components such as the X-ray sources, optical components, detectors and so on, performing high-sensitivity measurements even for tiny samples has been made possible. In this article, various examples of characterizations realized by the state-of-the-art “SmartLab  $\mu$ HR” diffractometer system, equipped with cutting-edge technologies, such as the ultra-high brilliance microfocus X-ray source, a magnificent optic system, combined with the multi-dimensional detector “HyPix-3000” are presented.

## 2. Features of SmartLab $\mu$ HR

### 2.1. Horizontal goniometer system

SmartLab  $\mu$ HR is a diffractometer system combining the goniometer of the general purpose SmartLab instrument with a microfocus rotating anode X-ray source and a CMF (Confocal Max-Flux) mirror as the

incident optic system (Fig. 1).

Since the goniometer holds the sample horizontally, it is easy to measure powders, liquids and bulky specimens without worrying about the sample falling. Moreover, by making use of optional attachments, it is possible to perform a mapping measurement of any location on the sample specified with a camera, or to make in-situ measurements by changing the atmosphere (temperature, humidity and so on) around the sample. In the following section, a detailed explanation is provided in regards to each technology and component that comprise the SmartLab  $\mu$ HR system.

### 2.2. X-ray source and CMF mirror

Sealed-tube and rotating anode generators are well known X-ray sources. In general, higher intensity can be achieved with the rotating anode type, for which higher input power can be set, than with the sealed-tube X-ray source.

X-ray focus is categorized into two types: line focus or point focus (Fig. 2). For line focus, X-rays are taken off in the direction orthogonal to the longitudinal direction of the focal profile on an X-ray target. This focus type is employed as the incident X-rays for measurement with para-focusing optics, parallel beam optics and so on. In the case of point focus, X-rays are taken off in the longitudinal direction (end-on) of the focal profile so that the projected cross-section of the X-rays can be arranged to have an equi-dimensional shape.

As the X-ray source of SmartLab  $\mu$ HR, the microfocus rotating anode X-ray source “RA-Micro7”

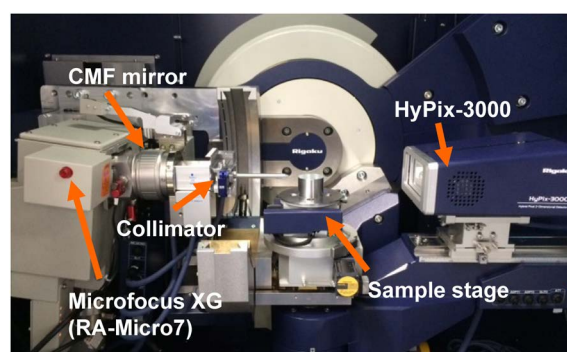


Fig. 1. SmartLab  $\mu$ HR.

\* Application Laboratories, Rigaku Corporation.

with point focus geometry is used, which realizes the world's highest level of power loading density at  $18\text{ kW/mm}^2$  with the electric power supply of  $800\text{ W}$  and the focal size of  $\phi 0.07\text{ mm}$ . The diverging X-ray beam emitted from this X-ray source is condensed and collimated by a focusing optical element, the "CMF mirror,"<sup>(1)-(6)</sup> and formed into a  $1.2\text{ mm} \times 1.2\text{ mm}$  beam that has a divergence angle collimated to approx.  $0.05^\circ$  in both directions orthogonal to the forward direction of the beam, as shown in Fig. 3. By employing a collimator and a pinhole in combination with a CMF mirror, a beam of

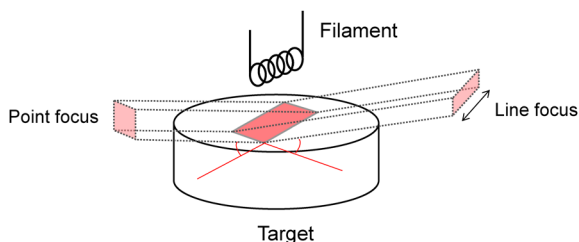


Fig. 2. Geometrical configuration of take-off directions for point focus and line focus.

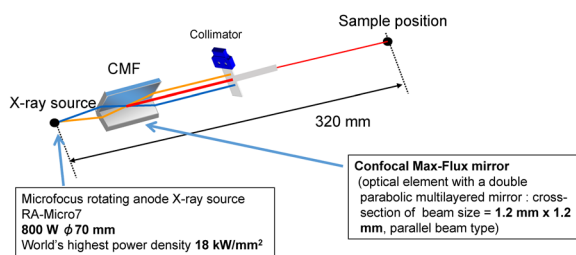


Fig. 3. Example of incident optical system configuration of SmartLab  $\mu$ HR.

$\phi 0.05\text{ mm} - 1.2\text{ mm}$  can be easily created.

By combining these X-ray source and optical elements, X-rays with significantly higher brilliance and improved collimation compared to the conventional equipment can be obtained. The name "MicroMax-007" is given to the X-ray generating system that consists of a combination of the "RA-Micro7" microfocus X-ray source and "Confocal Max-Flux" optics.

The results of intensity comparisons between SmartLab (line focus) and SmartLab  $\mu$ HR (point focus) with a  $\phi 0.05\text{ mm}$  collimator are shown in Fig. 4. This demonstrates that the intensity obtained by SmartLab  $\mu$ HR is about 100 times greater than that obtained from SmartLab with the same power loading.

### 2.3. Hybrid multi-dimensional pixel detector HyPix-3000

The HyPix-3000 is a hybrid multi-dimensional

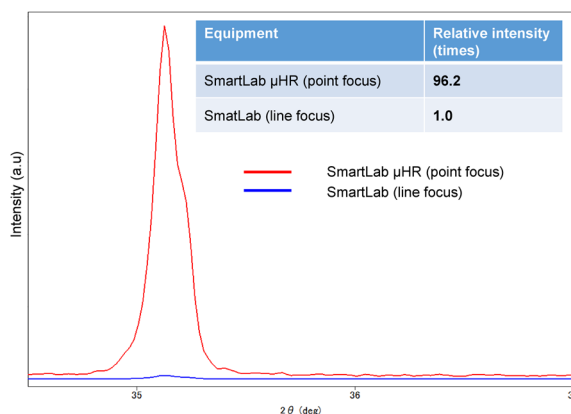


Fig. 4. Comparison of intensity between SmartLab and SmartLab  $\mu$ HR.

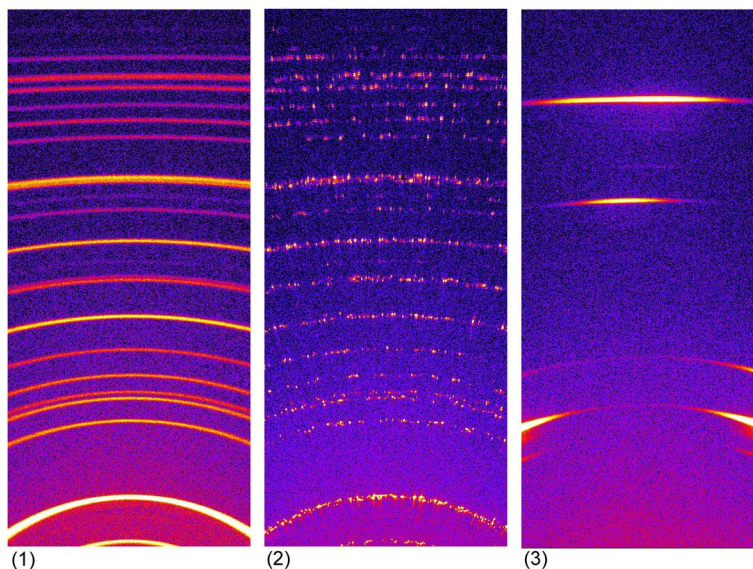


Fig. 5. Comparison of Debye rings.  
 (1) Quartz (particle size:  $10\ \mu\text{m}$ ).  
 (2) Quartz (particle diameter:  $100\ \mu\text{m}$ ).  
 (3) Aluminum (rolled plate).

pixel detector with a large effective detection area of approximately 3000mm<sup>2</sup> which enables measurement in 0D, 1D and 2D modes<sup>(7)-(9)</sup>. Thanks to the spatial resolution of the detector, the shape of Debye rings can be directly observed by measurement in 2D mode. Therefore, preferred orientation texture and coarseness of crystallites in a sample can be easily understood. An example of measurement of samples in different conditions is shown in Fig. 5. Uniform Debye rings are observed with a sample that has sufficiently fine grain size (Fig. 5(1)) and, on the other hand, discontinuous Debye rings consisting of dispersed spots are observed with the sample with coarse grain size (Fig. 5(2)). Moreover, with samples having a preferred orientation texture, Debye rings are observed as arcs rather than continuous rings (Fig. 5(3)).

The HyPix-3000<sup>(7),(9)</sup> is a detector with the many splendid features such as:

- \* Low background
- \* High-speed measurement with zero dead time
- \* Variable measuring mode (0D, 1D and 2D)

So far, the exposure method (snapshot) with the detector at a fixed position has been mainly used for measurements using two-dimensional detectors. However, the HyPix-3000 can perform TDI (Time Delay Integration) measurement<sup>(10)</sup> in 2D mode as well as in 1D mode. As a result, even for measurements that require collection of two-dimensional information over a wide range, the HyPix-3000 enables collecting signals by conducting TDI measurement in 2D mode; therefore, it makes obtaining high-quality data in a short time possible.

When  $2\theta/\theta$  measurement is performed in this measuring mode, it is possible to obtain information from the lattice plane nearly parallel to the sample surface (Fig. 6(1)). With the exposure measurement as

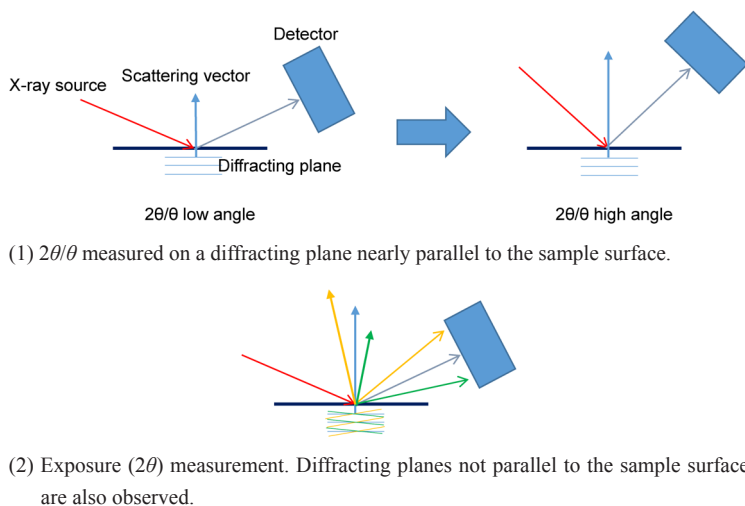


Fig. 6. Schematic drawing of  $2\theta/\theta$  and  $2\theta$  (exposure) measurement using 2D detector.

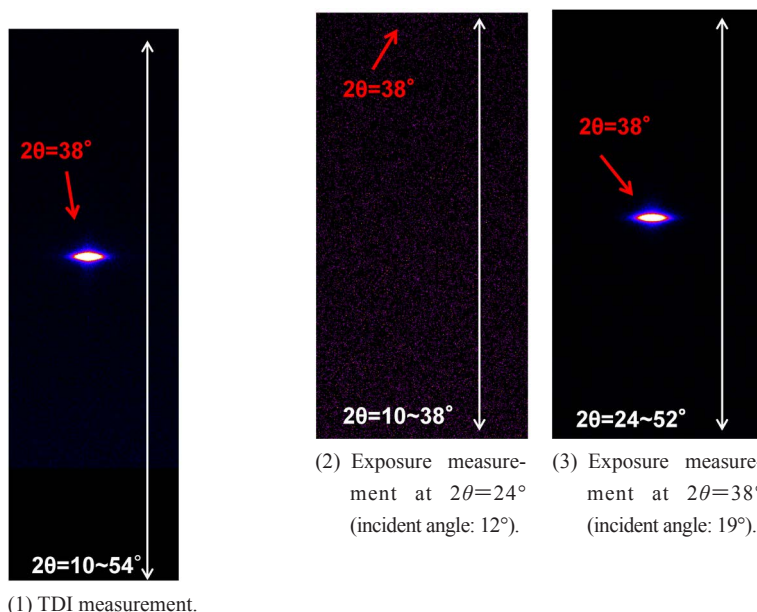


Fig. 7. TDI ( $2\theta/\theta$ ) measurement and exposure ( $2\theta$ ) measurement of Au thin film on Si substrate.

schematically shown in Fig. 6(2), since the observed lattice planes satisfying the diffraction conditions are greatly tilted from the sample surface for the diffraction signals at higher or lower  $2\theta$  positions, it should be noted that some peaks for samples with preferred orientation textures may be missed. An example is shown in Fig. 7. This sample is Au thin film with (111) preferred orientation texture grown on Si substrate. With TDI ( $2\theta/\theta$ ) measurement, the incident angle varies continuously, while the  $2\theta/\theta$  coupling scan enables observation of a diffracting plane nearly parallel to the surface (Fig. 7(1)). On the other hand, with exposure ( $2\theta$ ) measurement, because a lattice plane that satisfies the diffraction condition for Au111 does not exist for a certain fixed incident angle, no diffraction peaks might be observed in some cases (Fig. 7(2), (3)). Therefore, it should be noted that, with exposure measurement of samples with preferred orientation textures, the diffraction peak might not be observed for some incident angles in exposure ( $2\theta$ ) measurements.

As shown above, performing 2D-TDI measurement mode with the HyPix-3000 leads to the same result as measurements using multiple detectors that measure and collect the intensities simultaneously; therefore, it enables measurement in a short time compared to a 0D detector. This feature also impacts the measurement of a limited micro region on a sample surface. For 2D-mode measurement, which generally requires a point-shaped beam, the system combining the SmartLab  $\mu$ HR and HyPix-3000 may be regarded as the best match.

### 3. Examples of Measurement

#### 3.1. Evaluation of preferred orientation texture of Au thin film by mapping measurement

With the regular X-ray diffraction method, averaged information within an area is obtained when a large incident X-ray beam is employed. On the other hand, by limiting the size of the incident X-ray beam, it is possible to obtain local information about the sample. In the presented case, by using a  $\phi 0.05$  mm collimator, mapping measurement on 289 points within the area of  $1.7\text{ mm} \times 1.7\text{ mm}$  by  $0.1\text{ mm}$  step was performed for the Au thin film sample on Si substrate. Then the variation of the degree of preferred orientation was evaluated.

The measurement was performed with an exposure time of 5 seconds per point. During the mapping measurement, it is possible to capture an image of the sample by combining the measuring software "SmartLab Guidance" with a sample monitoring camera to designate the location of measurement. An example of a two-dimensional diffraction image of Au111 reflection is shown in Fig. 8. From this data, the intensity profile as a function of tilt ( $\beta$ ) direction ( $\beta$ - $I$  profile: Fig. 9) is derived, and the peak width at each measurement point was calculated. The mapping display of the result is shown in Fig. 10.

It is revealed that the sample has a variation of peak width (FWHM) ranging from  $1.58^\circ$ – $1.69^\circ$  depending on the location, and that the FWHM is slightly larger at the

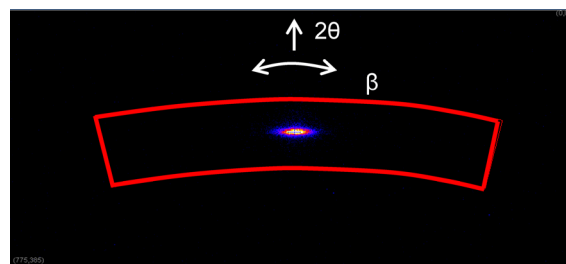


Fig. 8. Two-dimensional diffraction image of 111 reflection of Au thin film on Si substrate.

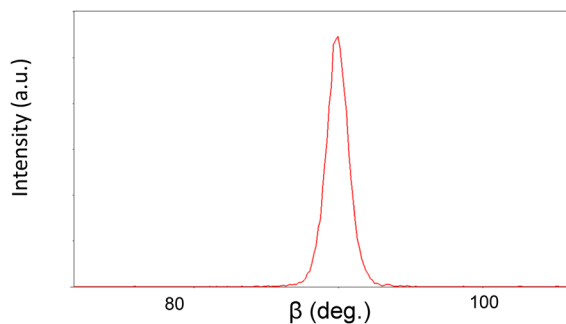


Fig. 9.  $\beta$ - $I$  profile of 111 reflection of Au thin film on Si substrate.

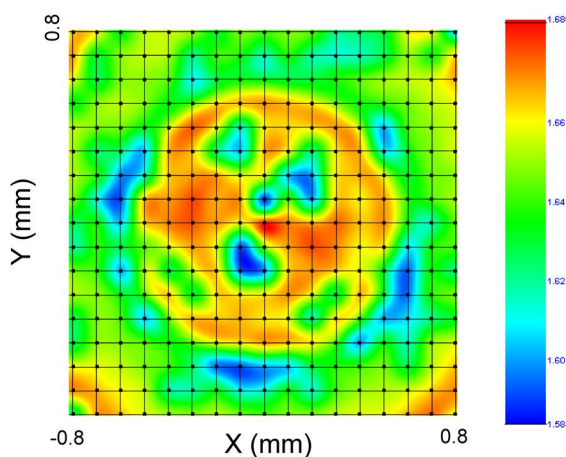


Fig. 10. Result of peak width distribution analysis for mapping data of 111 reflection of Au thin film on Si substrate.

center of the sample. Therefore, it is understood that the degree of preferred orientation texture for the Au thin film is relatively low in the center part of this sample.

For an identical characterization using a 0D detector instead of a 2D detector, it is necessary to perform rocking curve measurements ( $\omega$  scan) at each point. By combining a high-brilliance X-ray source and a 2D detector, it is possible to obtain information not only on tilt distribution (mosaic spread) but also on  $2\theta$ -direction simultaneously; therefore, a lot of information can be obtained by an exposure measurement in a short time even for a micro-area XRD measurement with weak or faint signals.

### 3.2. Phase ID analysis of a rock specimen by micro XRD measurement

Generally, the definition of a mineral is a naturally formed crystalline substance. A rock is an aggregate of minerals in which the crystallites tend to be small. Therefore, in order to perform a measurement of tiny mineral crystallites contained in rock, an optical system that can selectively measure the designated small area is required. For this measurement, by using a  $\phi$ 0.05 mm collimator, black and white areas of natural basalt rock specimen as shown in Fig. 11 are measured in approx. 40 minutes and, based on the resulting two-dimensional diffraction images, crystal phase identification analysis (identification of crystal phase) was performed.

In the two-dimensional diffraction image, discontinuous Debye rings composed of sparsely scattered spots are observed, therefore it is understood that the constituent crystallites are considerably coarse. Consequently, in order to increase the number of crystallites contributing to diffraction, the measurement was performed by oscillating the  $\phi$ -axis and the  $\chi$ -axis (tilt axis) (Figs. 12(1) and 13(1)).

For this experiment, TDI measurement in 2D mode

as described in section 2.3 was performed and, thanks to the large effective detection area of the HyPix-3000 and as a result of sample oscillation, wide scale two-dimensional information was collected in a short time and the necessary data for crystal phase identification was obtained. As a result, it was revealed that the white area was composed mainly of forsterite ( $\text{Mg}$ -rich  $(\text{Mg},\text{Fe})_2\text{SiO}_4$ ) and the black area was composed mainly of enstatite ( $\text{Mg}$ -rich  $(\text{Mg},\text{Fe})\text{SiO}_3$ ) (Figs. 12(2) and 13(2)).

As seen in Fig. 12(1), forsterite—which makes up the white area—has a considerably large particle crystallite size, therefore only discontinuous Debye rings composed of scattered spots are observed in the two-dimensional diffraction image. However, in the 1D profile derived from wide-scale two-dimensional information (Fig. 12(2)), a substantial number of diffraction peaks were observed and, thus the phase identification was successful.

On the other hand, the 1D profile of the black area resembles the diffraction pattern of a powder sample more than the white area and, at the same time, the two-dimensional diffraction image is composed of diffraction

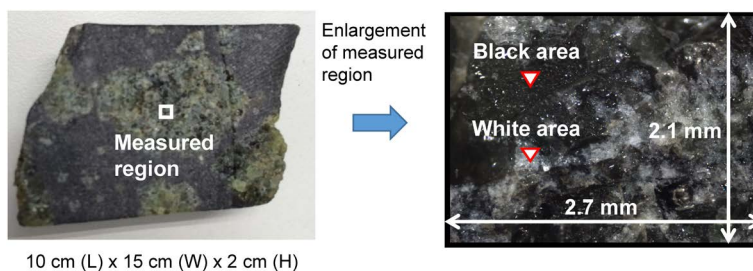


Fig. 11. Photographs of basalt rock specimen.

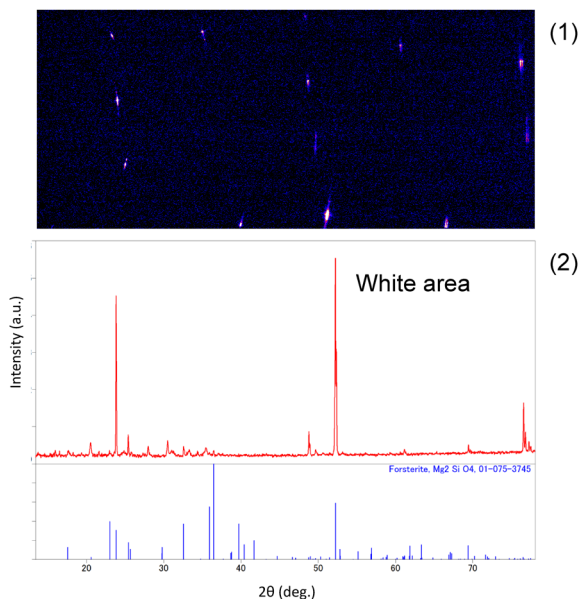


Fig. 12. (1) Two-dimensional diffraction image of white area by measurement with oscillation.  
(2) Result of qualitative analysis of white area.

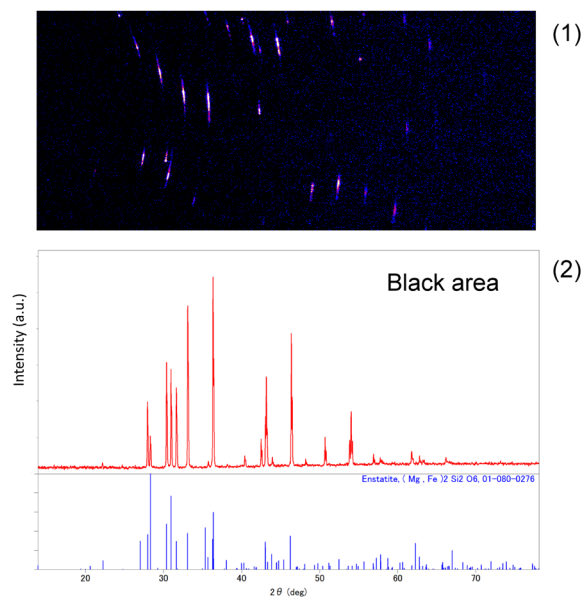


Fig. 13. (1) Two-dimensional diffraction image of black area by measurement with oscillation.  
(2) Result of qualitative analysis of black area.

arcs rather than sparsely scattered spots. This leads to the conclusion that the black area is composed mainly of randomly oriented or weakly textured enstatite crystals with relatively small crystallite sizes. For micro-area XRD analysis for small regions not composed of polycrystals but of a single crystal or a small number of crystallites, it is expected that the SmartLab  $\mu$ HR+HyPix-3000 system will powerfully assist these measurements and analyses.

### 3.3. Analysis of textured polypropylene by 2D-WAXS and 2D-SAXS

Polypropylene, a thermoplastic polymer produced by polymerizing propylene, is widely used as plastic containers for packaging material and so on. Differences in the heat treatment process may lead to a variety of orientation textures and higher order structure that, as a result, affect the property of the material.

For this reason, it is important to characterize this material or its composite substances by two kinds of measurements; namely, the analysis of texture of the molecular structure by WAXS and the analysis of higher order texture and long range order structure by SAXS. Due to the characteristics of organic material, measurement by the transmission method is effective. With SmartLab  $\mu$ HR, measurement of transmission 2D-WAXS and 2D-SAXS by utilizing the large effective area of the HyPix-3000 is available, therefore this requirement can be satisfied. By setting the camera length to 27 mm, exposure measurement of 2D-WAXS for the range of  $2\theta=7.0^{\circ}$ – $55.5^{\circ}$  can be performed. Then, by setting the camera length to 300 mm, measurement of 2D-SAXS for the range of  $2\theta=0.2^{\circ}$ – $7.0^{\circ}$  can be performed.

In this section, results of characterization of two kinds of polypropylene are presented.

The first one is of polypropylene films with stretching treatment. For uniaxially and biaxially stretched polypropylene films (approx.  $20\text{ mm} \times 20\text{ mm} \times 0.1\text{ mm}$ ), two-dimensional diffraction images by 2D-WAXS measurement with a camera length of 27 mm and an exposure time of 3 minutes are shown in Fig. 14. The orientation relationship between the directions of the stretching treatment of the sample and the incident X-rays is schematically shown in Fig. 15.

A two-dimensional diffraction image of uniaxially stretched film is shown in Fig. 14(1). It is clearly seen that reflections such as 110, 040 and 130 are observed mostly in the TD direction. On the other hand, from the two-dimensional diffraction image of biaxially stretched film (Fig. 14(2)), it can be easily understood that the distribution of 110 reflections shows the maximum of four peaks in the direction of MD and TD, therefore it has a different orientation texture from the uniaxially stretched sample. The degree of orientation texture can be evaluated by calculating the peak width of these peaks in the  $\beta$ -direction of the 110 reflection of each polypropylene film (Fig. 16).

The second example is a polypropylene plate.

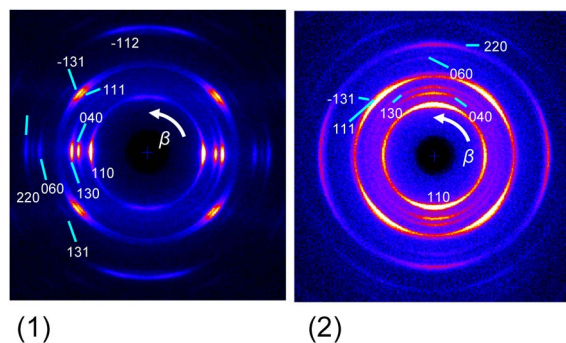
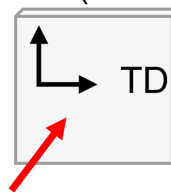


Fig. 14. Result of 2D-WAXS measurement of uniaxially and biaxially stretched polypropylene film.

(1) Uniaxially stretched film.

(2) Biaxially stretched film.

MD (Mechanical Direction)



TD (Traverse Direction)

X-ray incident direction

Fig. 15. The orientation relation between the directions of stretching treatment of the sample and incident X-rays.

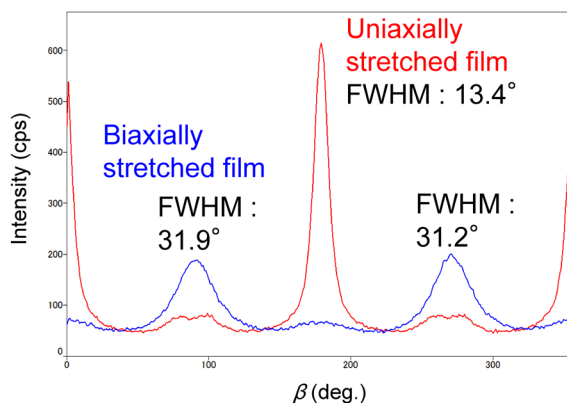
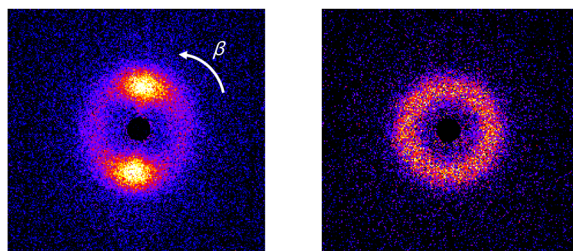


Fig. 16.  $\beta$ -I profile of 110 reflection of polypropylene films.

The two-dimensional diffraction images of a press molded polypropylene flat plate (approx.  $20\text{ mm} \times 20\text{ mm} \times 2\text{ mm}$ ) by 2D-SAXS measurement with a camera length of 300 mm and an exposure time of 60 and 90 minutes are shown in Fig. 17.

While Debye rings with uniform intensity are observed in the two-dimensional diffraction image of press molded polypropylene flat plate shown in Fig. 17(2), the intensity of Debye rings in the two-dimensional diffraction image of polypropylene flat plate without press molding shown in Fig. 17(1) is not uniform and two maxima are observed. By comparing



Exposure time: 60 minutes

Exposure time: 90 minutes

**Fig. 17.** Result of 2D-SAXS measurement of polypropylene flat plates.

- (1) Polypropylene flat plate.
- (2) Polypropylene flat plate (press molded).

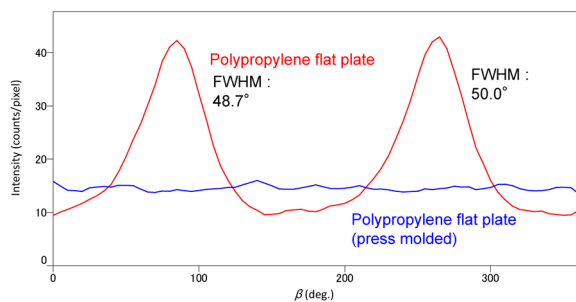


**Fig. 18.**  $\beta$ - $I$  profile of polypropylene flat plates for long-range order peak.

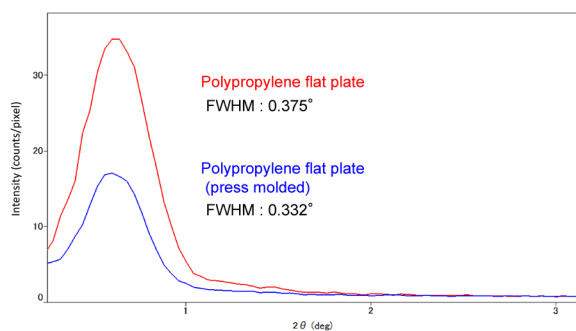


**Fig. 19.**  $2\theta$ - $I$  profile of polypropylene flat plates.

these two-dimensional diffraction images, the apparent difference in preferred orientation texture of long-range order structure within surface planes can be confirmed. Also, quantitative evaluation of the degree of preferred orientation texture of long-range order structure within surface planes can be evaluated as well from their

intensity distribution profiles in the  $\beta$ -direction (Fig. 18).

Additionally, as shown in Fig. 19, the length for long-range order structure can be calculated from peak positions in the  $2\theta$ -profile derived from the two-dimensional diffraction image, and the variation of their interplanar distances can be evaluated by calculating the peak width. The full width at half maxima (FWHM) of the peak for the press molded sample and the variation of their interplanar distances are found to be smaller than the one for the non-pressed sample

#### 4. Conclusion

The SmartLab  $\mu$ HR is equipped with state-of-art device technology and functional components, such as a high-brilliance X-ray source, a CMF mirror (producing a high-quality incident X-ray beam), a versatile goniometer system (horizontal sample holding, controlling software and so on), and the multi-dimensional detector HyPix-3000. By making the best of these assets, measurements that previously could only be performed at a synchrotron radiation facility can now be done in the home lab, along with complex evaluation methods that were difficult with conventional equipment<sup>(11)</sup>. With this system, the time required for material characterization should be considerably shortened, leading to a wider range of possibilities for new material development.

#### References

- (1) L. Jiang, B. Verman, B. Kim, Y. Pulatonov, Z. Al-Mosheky, R. Smith and N. Grupid: *Rigaku Journal (English version)*, **18** (2001), No. 2, 13–22.
- (2) L. Jiang, Z. Al-Mosheky and N. Grupid: *Powder Diffraction*, **17** (2002), 81–93.
- (3) B. Verman, L. Jian and B. Kim: *Rigaku Journal (English version)*, **19** (2002), No. 1, 4–13.
- (4) A. M. Z. Slawin and J. D. Woollins: *Rigaku Journal (English version)*, **22** (2005), No. 1, 26–30.
- (5) K. Shimizu and K. Omote: *Rigaku Journal (English version)*, **24** (2008), No. 1, 1–9.
- (6) Y. Ito: *Rigaku Journal*, **25** (2009), No. 1, 1–6.
- (7) *Rigaku Journal (English version)*, **30** (2014), No. 2, 38–40.
- (8) P. Maj, R. Szczygiel, P. Gryboś, T. Taguchi and Y. Nakaye: *J. Instrum.*, **10** (2015), C02006.
- (9) A. Ohbuchi: *Rigaku Journal (English version)*, **31** (2015), No. 1, 4–9.
- (10) S. Kobayashi and K. Inaba: *Rigaku Journal (English version)*, **28** (2012), No. 1, 8–13.
- (11) P. Zaumseil: *J. Appl. Cryst.*, **48** (2015), 528–532.